Photostabilization of polyethylene by a hindered amine light stabilizer in blooming conditions and impact of MDO processing

Julien Christmann [a], Jean-Luc Gardette [a], Gérard Pichon [b], Bruno Bouchut [b], Sandrine Therias [a,*]

[a] Université Clermont Auvergne-CNRS-Clermont Auvergne INP, ICCF F-63178 Aubière, France
[b] Barbier group, F-43600 Sainte-Sigolène, France

ABSTRACT

The effect of Machine Direction Orientation (MDO) processing on the photostabilization of LLDPE samples containing Tinuvin® 770 was studied. The amount of Tinuvin® 770 in the processed samples was deliberately chosen at a level higher than the reported solubility at ambient temperature for two main reasons: the first reason was to assess the equilibrium between the soluble and nonsoluble forms of this additive and the impact of the MDO process, and the second was to demonstrate the role of a higher temperature in accelerated artificial photoaging on the protective role played by the nonsoluble part. The results reported in this article show that at room temperature, a nonnegligible amount of Tinuvin® 770 precipitates at the surface, which is commonly termed blooming. However, the additive that bloomed at the surface can be dissolved within the polymer with increasing temperature, which is the case in the conditions of accelerated artificial photoaging but not the case of natural outdoor weathering. Such physical phenomena are responsible for a possible bias brought by temperature during accelerated photoaging, which can affect aging tests. This questions the representativeness of accelerated aging at higher temperatures for polymers containing a blooming stabilizer.

© 2021 Elsevier Ltd. All rights reserved.

1. Introduction

It is well established that polymers, such as polyethylene, are prone to degradation through an oxidative chain-radical mechanism upon exposure to external stress factors such as heat or UV light [1,2,3]. This leads to the production of oxidation products, such as ketones (further reacting by Norrish mechanisms), carboxylic acids, and aldehydes, and causes the modification of the polymer properties (especially mechanical and aesthetic properties) [3,4]. To prevent photodegradation during processing and subsequent service life, stabilizers (or antioxidants) and/or UV absorbers are generally added to the polymer formulation at concentrations of 0.01 to 1.0 wt%. Stabilizers are organic compounds readily able to slow oxidation reactions by reacting with key intermediates such as hydroperoxides and radicals. UV absorbers aim to protect the polymer from UV absorption and/or the stabilizers from direct photodegradation, which dramatically reduces their protective effect. To act efficiently, an additive must be incorporated in an active and soluble form.

The solubility of an additive within a polymer is actually governed by several factors [5,6]: the temperature, the intrinsic nature of the additive (its heat of fusion and melting point) and its interactions with the polymer (also referred to as their compatibility). It is also well documented that soluble additives are only present in the amorphous phase of polyolefins, as the crystalline areas are too densely packed for the additive to enter [7,8]. Because they are mainly based on functional groups such as phenols, amines, phosphites or sulfides, common stabilizers are polar molecules whose solubility in apolar polyolefins, such as polyethylene, is poor at ambient temperature [5,9].

Additives are generally introduced at concentrations far higher than room-temperature equilibrium concentrations. They are nevertheless fully soluble during polymer processing at high temperature due to the beneficial effect of temperature on the solubility. This results in supersaturation upon cooling and storage, which is an important factor in determining their service lifetime and has to be considered in accelerated aging tests [6]. Two phenomena can then be encountered: *i.* microprecipitation (formation of stabilizer nodules within the polymer, leading to microphase separation) and *ii.* blooming (surface segregation of the stabilizer through exudation). Low-weight (molecular) antioxidants are prone to blooming, as their diffusion coefficient within the polymer is higher [9]. In a
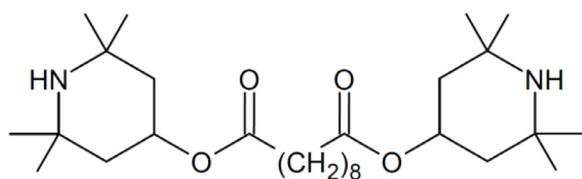
Fig. 1. Chemical structure of Tinuvin® 770.

Table 1
Tinuvin® 770 content and MDO draw ratio of PE samples.

Sample	wt% Tinuvin® 770	MDO draw ratio
PE-1	0	1 (undrawn)
PE-3	0	3
PE-770-1	0.3	1 (undrawn)
PE-770-3	0.3	3

recent paper, Xu et al. [10,11] studied the blooming of the molecular phenolic antioxidant Irganox 1076® at the surface of silane-crosslinked polyethylene.

Tinuvin® 770 is a low-weight Hindered Amine Light Stabilizer (HALS) used in polyolefins [9,12,13,14]. It contains two piperidyl rings separated by a sebacate ester functional group (Fig. 1). Its solubility in LDPE has been estimated to be 0.1 wt% at room temperature [9,12]. Progressive blooming from this polymer after high-temperature processing was studied by Zehnacker et al. [12].

Machine Direction Orientation (MDO) is a technology essentially employed for polyethylene (PE) and consists of uniaxially stretching a polymer film between consecutive hot and cold rolls to improve its properties while reducing the amount of matter necessary to reach them. More specifically, the process can be decomposed into four steps: preheating, stretching, annealing, and cooling [15,16]. First, heated rolls uniformly bring the polymer film to the desired temperature for stretching. Then, it is drawn between two rolls inversely rotating at different speeds (namely, the "slow" and "fast" rolls). The drawn film goes between heated rolls for thermal stabilization, especially for shrinkage ability. Finally, it is cooled at ambient temperature before winding. The draw ratio (DR or λ) corresponds to the ratio between the initial and final thicknesses of the film, which is mainly governed by the ratio of the speeds of the two drawing rolls. As the drawing temperature is below the melting point of the polymer, this process is referred to as a "cold-drawing" process. At the macromolecular scale, it causes the initial spherulitic morphology to progressively transform into a fibrillar morphology oriented along the machine direction (MD) as the drawing rate is increased [17]. Accordingly, the polymer optical (increase in gloss and transparency, decrease in haze) [18,19,20], mechanical (increase in the Young's modulus along the machine and transverse directions, as well as stress at break along the MD) [18–21] and barrier (gas, water vapor) [18,21] properties are enhanced. MDO technology was developed 50 years ago [22] and is widely used at the industrial scale. However, its effect on polymer properties remains confidential in the scientific literature [17–21,23,24], and its consequences on stabilizer solubility and polymer photoaging have never been considered thus far.

From a general point of view, the effect of polymer orientation (regardless of its origin) on additive solubility has scarcely been considered. Moisan studied the evolution of Irganox 1076® diffusion and solubility in oriented LDPE films [25]. Following an increase at a low draw ratio, the solubility was reported to decrease as the orientation increased. However, all the experiments were performed at temperatures higher than the melting point of the additive.

This paper aims to investigate the impact of the MDO process on the photostability of PE films containing Tinuvin® 770, with special concern for the protective role of the stabilizer precipitated at the surface (blooming) in accelerated photoaging tests. For this purpose, LLDPE films were deliberately processed at 0.3 wt% HALS, which is a concentration that can lead to supersaturation of the additive at room temperature. Tinuvin® 770 was first individually characterized, and its presence in the films was assessed by infrared spectroscopy. Reversible blooming of the stabilizer was evidenced by washing and thermal treatment, and quantification of the amount of soluble HALS was performed. One may question how much of the additive can be present in the polymer at equilibrium and how physical phenomena affect aging tests. Undrawn and MDO-stretched samples were compared with respect to their Tinuvin® 770 content. Finally, photoaging kinetics in conditions of accelerated artificial aging were obtained and discussed based on the effect of the MDO process on the stabilizer total content.

2. Experimental

2.1. Materials

The linear low-density polyethylene (hereafter denoted "PE-") was LLDPE BorShape™ FX 1001 grade supplied by Borealis [26]. Tinuvin® 770 (bis(2,2,6,6-tetramethyl-4-piperidyl) sebacate, m.p. = 81–83 °C [6,9,12]) was supplied by BASF. The ethanol (EtOH, 96 %) used for washing was purchased from VWR Chemicals. All products were used as received.

2.2. MDO processing

All PE films were provided by the Barbier group (Sainte-Sigolène, France). Reference films without Tinuvin® 770 and films stabilized with 0.3 wt% Tinuvin® 770 ("PE-770-") were prepared. Undrawn films (denoted by "-1") were processed by cast extrusion to a final thickness of 50 μm. Extrusion and MDO processing was performed at Omya (Oftringen, Switzerland) from cast-extruded films of 150 μm thickness. The heating step was performed at 90 °C, with subsequent annealing performed at 60°C before cooling at room temperature on water-cooled rolls. A final thickness of approximately 50 μm was obtained, corresponding to an MDO draw ratio of 3 (samples denoted by "-3"). A list of the PE samples is given in Table 1.

2.3. Irradiation

Photodegradation experiments were carried out in a SEPAP 12/24 unit [27] in the presence of air. This accelerated weathering device was equipped with 4 medium-pressure mercury lamps (400 W) emitting polychromatic light whose wavelengths lower than 300 nm are filtered by a borosilicate envelope. The delivered light intensity was 90 W m^{-2} in the wavelength range of 300–420 nm, and the chamber temperature was measured at 52 °C. For transparent PE samples, it is assumed that the sample temperature is close to this value.

2.4. Heating

Films were submitted to thermal treatment at 52 °C (same temperature as that of the irradiation device) in a forced convection oven from Binder.

2.5. Infrared spectroscopy

Infrared spectra were recorded between 4000 and 400 cm^{-1} in the transmission mode with a Nicolet 6700 FTIR spectrometer

(ThermoFisher) equipped with a DTGS-KBr detector and operated with OMNIC software. The analysis chamber was maintained under a dry atmosphere by the continuous purging of dry air. Each spectrum was obtained by the accumulation of 32 scans with a 2 cm^{-1} resolution. When necessary, FTIR spectra can be normalized by the absorbance of the 1378 cm^{-1} band (symmetric bending of end-of-chain –CH$_3$ groups).

FTIR spectroscopy was also performed in single reflection Attenuated Total Reflection (ATR) mode between 4000 and 600 cm^{-1} with two types of crystals (Ge and diamond). For the former, a Nicolet IS10 spectrometer (ThermoFisher) equipped with a Smart OMNI-Sampler accessory (ThermoFisher) was used (64 scans, 4 cm^{-1} resolution). For the latter, a Nicolet 380 apparatus coupled with a Golden Gate ATR modulus (Specac) was employed (64 scans, 4 cm^{-1} resolution).

In ATR mode, the penetration depth D$_p$ of the IR beam depends on its wavelength according to Eq. 1 [28].

$$D_p = \frac{\lambda}{2\pi\sqrt{n_1^2 \sin\left(\theta\right)^2 - n_2^2}} \tag{1}$$

In this equation, λ is the wavelength, n_1 is the ATR crystal refractive index (4.0 for Ge, 2.4 for diamond), θ is the angle of incidence of the IR beam (45° for the apparatus used), and n_2 is the sample refractive index (1.51 for PE [29]). For instance, the penetration depth in the 1700 and 1800 cm^{-1} region ranges between 0.37 and 0.39 μm for a Ge crystal and is 1.19–1.26 μm for a diamond crystal. Spectra were corrected for the variation in D$_p$ with wavelength, as well as the shifting of absorption bands, with the advanced ATR correction function of OMNIC software.

FTIR mapping was realized with a Spectrum 100 spectrometer (PerkinElmer) coupled with a Spotlight 400 imaging system (PerkinElmer). In transmission mode, images of 350 × 350 μm dimensions (56 × 56 pixels, 6.25 × 6.25 μm per pixel) were recorded between 4000 and 650 cm^{-1} (128 scans per pixel, 4 cm^{-1} resolution). ATR mapping was performed with a Ge crystal to obtain images of 300 × 300 μm dimensions (192 × 192 pixels, 1.56 × 1.56 μm per pixel) between 4000 and 720 cm^{-1} (8 scans per pixel, 4 cm^{-1} resolution).

2.6. UV–visible spectroscopy

UV–visible spectra of polymer films were recorded with a Shimadzu UV-2600 scanning spectrophotometer equipped with an ISR-2600 Plus integration sphere unit and operated with UVProbe software. Acquisition was performed at a scan speed of 500 nm/min ("slow" mode) with a 5 nm slit width and 2 nm data interval.

Fig. 3. FTIR transmission spectra of PE-770-1 (blue) and PE-770-3 (red) in the 1900–1500 cm^{-1} region. (For interpretation of the references to color in this figure legend, the reader is referred to the web version of this article.)
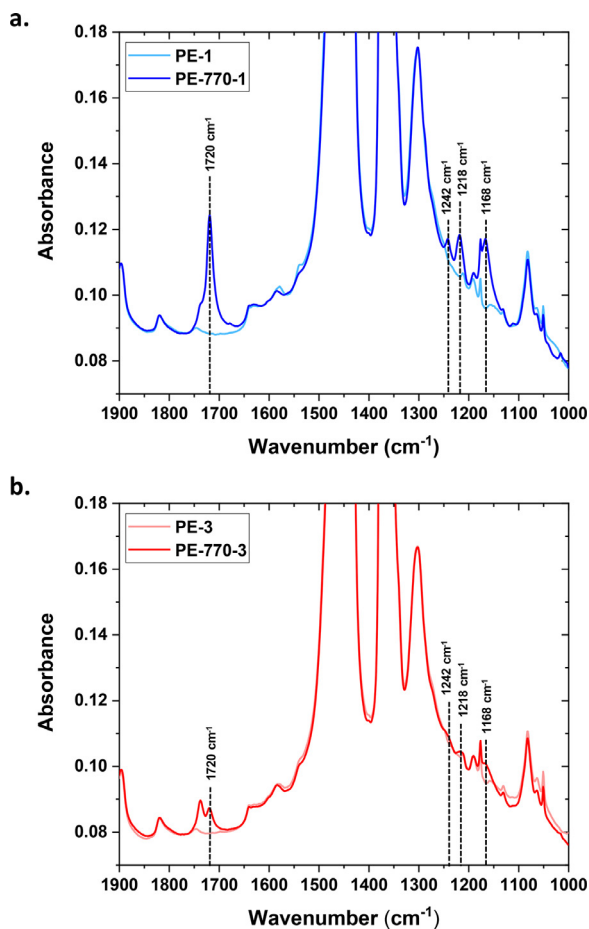

Fig. 2. FTIR transmission spectra of a. undrawn samples PE-1 (light blue) and PE-770-1 (blue) and b. MDO-drawn samples PE-3 (light red) and PE-770-3 (red). (For interpretation of the references to color in this figure legend, the reader is referred to the web version of this article.)
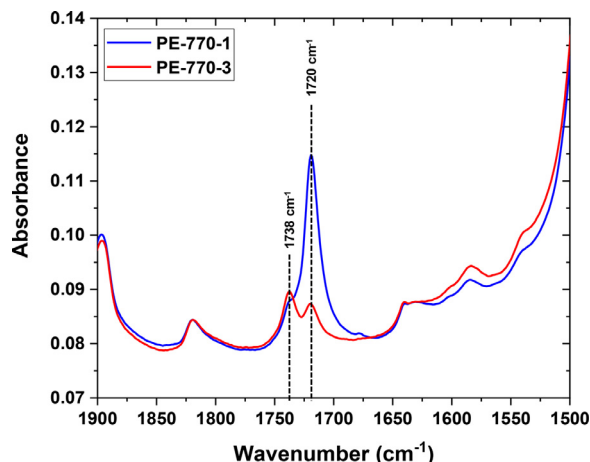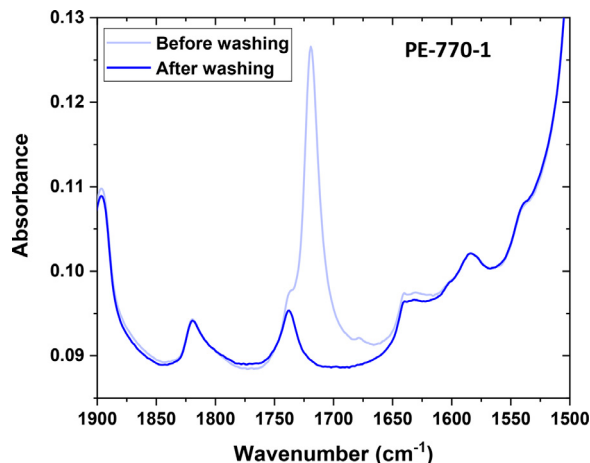

Fig. 4. FTIR transmission spectra of PE-770-1 before (light blue) and after (blue) washing with EtOH and overnight drying. (For interpretation of the references to color in this figure legend, the reader is referred to the web version of this article.)
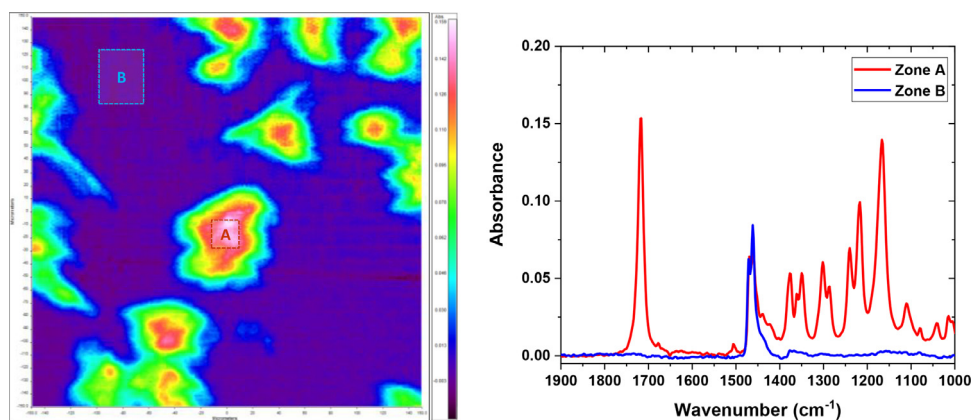
Fig. 5. FTIR ATR mapping image (300 × 300 μm) of PE-770-1 recorded at 1720 cm^{-1} (left) and spectra taken in the A and B zones identified in the mapping image (right). Each pixel is of 1.56 × 1.56 μm dimensions.

Fig. 6. SEM images (× 400) of unwashed (left) and EtOH-washed (right) PE-770-1 films.

2.7. SEM imaging

SEM images were recorded with a SEM-FEG Supra 55VP microscope from Zeiss. Samples were metallized with Au prior to secondary electron imaging in a high vacuum (7 × 10^{-7} Torr) at 10 kV.

2.8. Thermal analysis

Differential Scanning Calorimetry (DSC) was performed with an 822e apparatus from Mettler Toledo. Samples (between 11 and 18 mg) were introduced into an aluminium crucible and subjected to a heating-cooling-heating cycle from -20 to 160 °C at a rate of 10 °C/min under a dry air atmosphere. The crystallinity rate was estimated from the ratio of the melting enthalpy of the sample to that of a 100% crystalline PE sample (293 J g^{-1} [30]). Data from the first heating step were used to consider the thermal history of the sample.

3. Results and discussion

3.1. Characterization of Tinuvin® 770 in the PE films

FTIR spectra of pure Tinuvin® 770 were recorded in transmission (dispersed in a KBr tablet) and ATR modes (diamond and Ge, Fig. S1). Several absorption bands characteristic of the functional groups of Tinuvin® 770 can be identified at 3320 cm^{-1} (N-H symmetric stretching), 1720 cm^{-1} (C=O symmetric stretching), 1242 cm^{-1} and 1218 cm^{-1} (superposition of several vibrations, especially N-H out-of-plane bending, C-N stretching and CH$_2$ deformation) and 1168 cm^{-1} (piperidyl ring asymmetric stretching and sebacate ester C-O asymmetric stretching) [12,31–33].

FTIR transmission spectra of PE films stabilized with Tinuvin® 770 were recorded for the undrawn PE-770-1 (Fig. 2a) and MDO-drawn PE-770-3 films (Fig. 2b). For comparison, the spectra of the pristine PE films (PE-1 and PE-3) are superimposed. It can be observed that additional bands corresponding to those reported above for the stabilizer are present.

Enlarging the spectra between 1900 and 1500 cm^{-1} (Fig. 3) reveals the presence of an extra signal located at 1738 cm^{-1}, either as a shoulder for PE-770-1 or a band for PE-770-3. This has been attributed by Zehnacker et al. [12] to the C=O symmetric stretching of Tinuvin® 770 dissolved in LDPE. According to the spectra
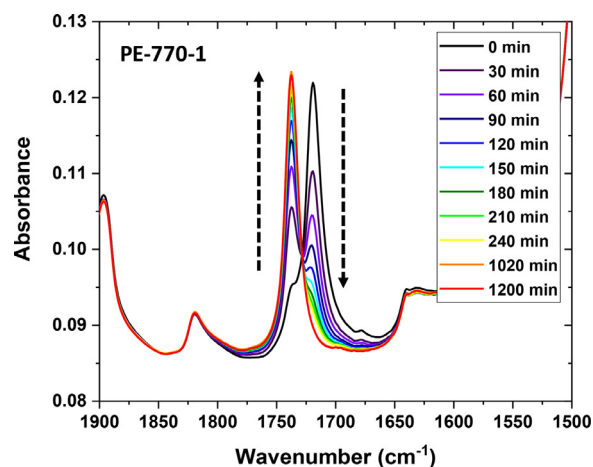

Fig. 7. FTIR transmission spectra of PE-770-1 before (black) and after various durations of heating at 52 °C. The arrows indicate the evolution with increasing heating duration.

of pure Tinuvin® 770, the 1720 cm^{-1} band is associated with its undissolved form (*vide infra*). The presence of two bands suggests that there is an equilibrium between dissolved and undissolved Tinuvin® 770 in the PE samples. This is not surprising, as the amount of stabilizer initially introduced into the polymer formulation during film processing (0.3 wt%) is higher than its reported solubility in LDPE at ambient temperature (0.1 wt%) [9,12]. The insoluble part of Tinuvin® 770 would then progressively bloom at the surface of the films during cooling and storage.

Although Tinuvin® 770 is not the best commercially available HALS for PE, it can be used as an efficient probe for studying blooming and for highlighting solubility differences upon MDO processing. Indeed, it can be observed in Fig. 3 that the equilibrium between soluble and nonsoluble HALS is affected by MDO processing, which will be discussed later.

3.2. Evidence of Tinuvin® 770 blooming at the PE surface

An easy way to experimentally demonstrate blooming consists of washing the sample films with a solvent of the stabilizer that is not a solvent of the polymer. Ethanol was chosen, and PE-770-1 and PE-770-3 films were briefly washed by spraying and then dried overnight. FTIR transmission spectra were recorded before and after washing (Fig. 4 for PE-770-1, Fig. S2 for PE-770-3). They show a general decrease in the absorbance of the Tinuvin® 770 characteristic bands. It is worthy to note a total disappearance of the 1720 cm^{-1} band, while the band at 1738 cm^{-1} remains unaltered. The complete disappearance of the band at 1720 cm^{-1} indicates that Tinuvin® 770 located at the surface of the films was removed by washing.

To further assess the presence of bloomed Tinuvin® 770 at the surface of the samples, FTIR ATR mapping was performed for a PE-

770-1 film and plotted at 1720 cm^{-1} (Fig. 5, left). Particles of tens of microns in size with a strong absorbance at this wavenumber are distributed at the film surface (according to Eq. 1, the penetration depth at 1720 cm^{-1} is less than 0.5 µm). Spectra recorded at the location of the absorbing particles (Fig. 5, right) show the presence of the other bands reported for Tinuvin® 770 (*vide supra*), and these particles can then be confidently identified as bloomed Tinuvin® 770 heterogeneously distributed at the film surface.

This observation was confirmed by comparing SEM images recorded for unwashed and EtOH-washed PE-770-1 films (Fig. 6). Several micrometre-sized particles are distributed at the surface of the unwashed sample but are totally absent from the washed sample. These experiments unambiguously confirm that a nonnegligible amount of Tinuvin® 770 blooms at the surface of the PE samples.

PE-770-1 films were then submitted to thermal treatment at 52 °C for 20 h, and transmission FTIR spectra were recorded at different time intervals (Fig. 7). Such a temperature was selected because it enables smooth heating (below the Tinuvin® 770 melting point) and corresponds to the actual temperature within the accelerated photoaging setup thereafter used (*vide infra*). The 1720 cm^{-1} band progressively decreases in intensity for the benefit of the 1738 cm^{-1} band, which is interpreted as a progressive solubilization of the bloomed HALS. This was confirmed by the disappearance of the micron-sized bloomed Tinuvin® 770 particles upon the same thermal treatment, as shown in the SEM images (Fig. S3). A similar experiment performed on pristine PE-1 showed that no thermooxidation of PE was observed within this range of time. From the variations in the absorbance at 1738 cm^{-1}, it is possible to estimate the amount of bloomed Tinuvin® 770, which is thermally re-solubilized (Fig. S4). More than 90% of bloomed Tinuvin® 770 can be re-solubilized within the first 4 hours. This con-
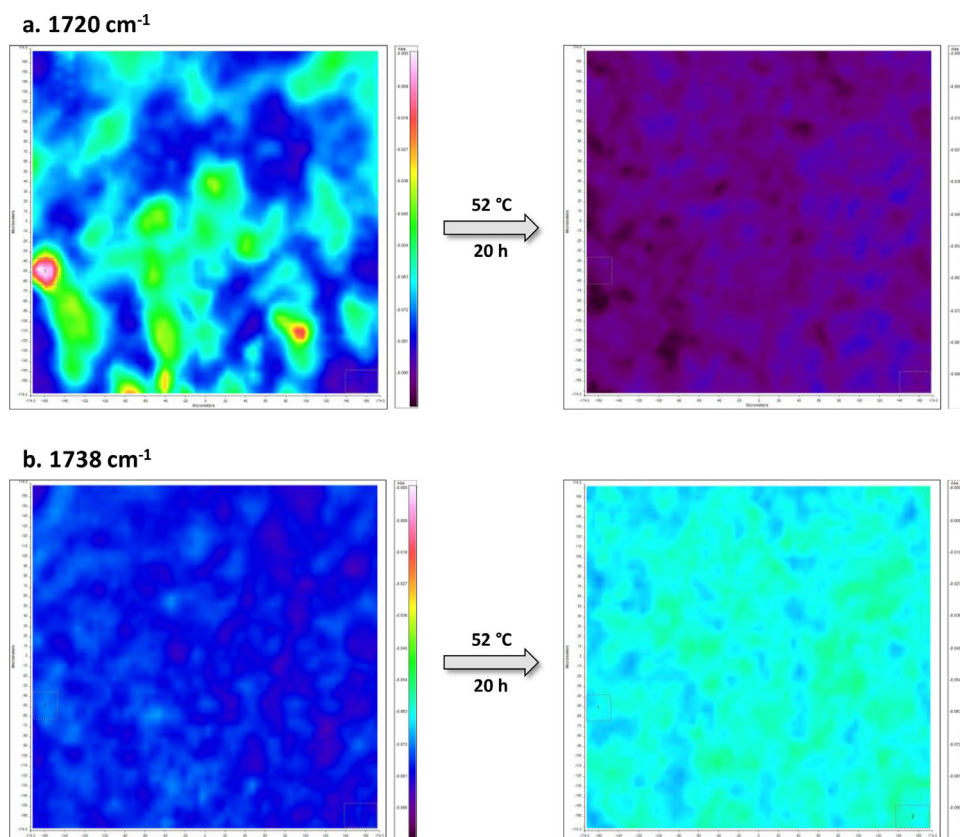

Fig. 8. FTIR transmission mapping image (350 × 350 µm) of PE-770-1 recorded at a. 1720 cm^{-1} before (left) and after (right) heating and b. at 1738 cm^{-1} before (left) and after (right) heating. Each pixel is of 6.25 × 6.25 µm dimensions.

firms former results reporting that the blooming of Tinuvin® 770 is thermally reversible [12]. Experiments run at higher temperatures (namely, 60 and 100 °C) showed a similar but faster process. Note that similar observations were made for PE-770-3 films after EtOH washing and thermal treatment.

FTIR transmission mapping of PE-770-1 was performed at 1720 and 1738 cm^{-1} before and after thermal treatment to assess the distribution of bloomed and solubilized Tinuvin® 770 respectively (Fig. 8). The distribution of the stabilizer within the depth was not considered here.

The mapping image at 1720 cm^{-1} shows that bloomed particles are heterogeneously distributed before heating and totally disappear after it (Fig. 8a), in accordance with the previous reported observations. In addition, a homogeneous distribution of HALS is observed in the image at 1738 cm^{-1} after solubilization of the bloomed particles (Fig. 8b). Solubilized Tinuvin® 770 is then homogenously distributed within the polymer rather than preferentially located close to the original position of the bloomed particles, which indicates that it can diffuse into the polymer.

Upon storage at ambient temperature, the opposite effect is observed (Fig. S5), with a progressive blooming of the stabilizer at the film surface. However, note that the associated kinetics are far slower. The reported results clearly show that the solubilization/blooming of Tinuvin® 770 is a thermally activated and reversible process. In addition, the easy experimental distinction between its soluble and bloomed forms from the 1738/1720 cm^{-1} bands observed by FTIR spectroscopy makes Tinuvin® 770 a good probe for the HALS blooming/re-solubilization phenomenon and its consequences during accelerated photoaging.

3.3. Quantification of soluble Tinuvin® 770 in samples

Quantification of soluble Tinuvin® 770 from FTIR spectra can be performed using Eq. 2:

$$wt\%_{soluble} = \frac{A_{1738}\ M_{770}}{2\ \varepsilon_{1738}\ l\ \rho_{PE}} \times 100 \qquad (2)$$

In this equation, A_{1738} and ε_{1738} are the absorbance and the molar absorption coefficient of Tinuvin® 770 at 1738 cm^{-1}, respectively, M_{770} is the molar mass of Tinuvin® 770 (expressed in kg·mol^{-1}), l is the thickness of the polymer film, and ρ_{PE} is the density of the studied PE film (0.931 Kg L^{-1} [26]). Factor 2 in the equation considers the fact that there are 2 ester functional groups per molecule of Tinuvin® 770.

The literature indicates a value of 580 L mol^{-1} cm^{-1} for the molar absorption coefficient at 1738 cm^{-1} of Tinuvin® 770 [9]. The amount of Tinuvin® 770 was calculated after complete thermal solubilization in PE-770-1 samples (*vide supra*). An average value of 0.28 ± 0.1 wt% was obtained from experiments performed for 8 samples. This value reflects the quantity initially introduced during the processing of the samples (0.3 wt%). Our results indicate that no (or at least only a negligible part of) Tinuvin® 770 is lost through evaporation during re-solubilization, which seems reasonable considering the low temperature used (52°C) and short heating time (20 h).

The same calculation was made to obtain the amount of soluble Tinuvin® 770 at ambient temperature after EtOH washing. Values of 0.05 and 0.08 wt% were found for PE-770-1 (8 samples) and PE-770-3 (10 samples), respectively. This suggests that the amount of soluble Tinuvin® 770 in both films is lower than the reported solubility (0.1 wt%) [9,12] and is also affected by MDO processing.

3.4. Impact of the MDO process on Tinuvin® 770 solubility in PE

As seen in Fig. 3, there are strong differences in the 1720/1738 cm^{-1} ratios of the undrawn and MDO-drawn samples.
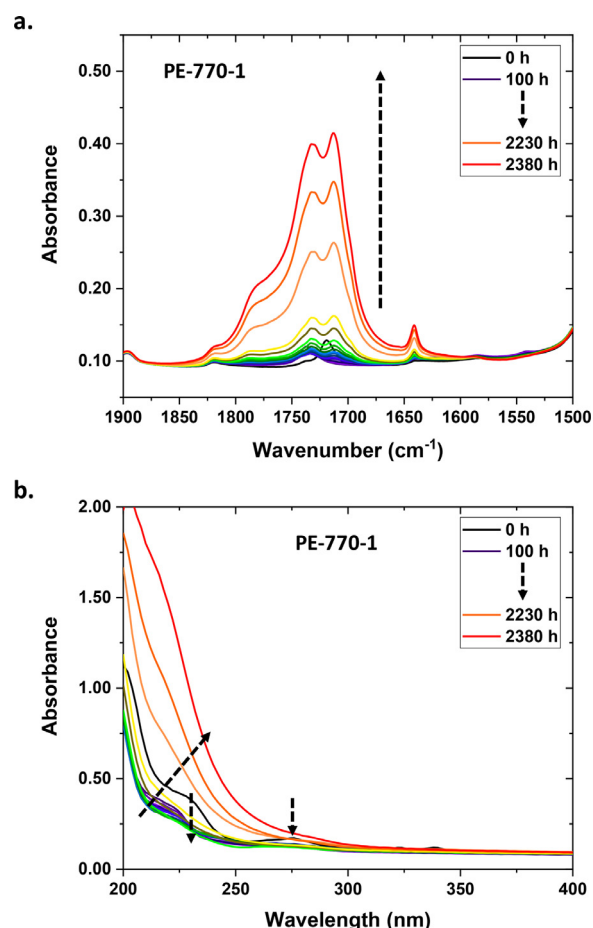

Fig. 9. a. FTIR transmission spectra in the 1900-1500 cm^{-1} region and b. UV–visible spectra of PE-770-1 after various photoaging durations. The arrows indicate the evolution with increasing UV exposure time.

Indeed, the ratio strongly favours the 1720 cm^{-1} band (bloomed form) for PE-770-1, while it is more equilibrated for PE-770-3. In addition, PE-770-1 appears to contain far more bloomed HALS, while PE-770-3 contains more of the soluble form (*vide supra*). The overall content of Tinuvin® 770 is then finally higher for the undrawn sample.

DSC experiments reveal that the crystallinity rates of the original and drawn samples are similar (approximately 47 % for both of them). The increase in the soluble content observed for the MDO-processed samples is thus independent of the crystallinity rate. It would rather originate from the MDO process itself, which also leads to a strong decrease in the bloomed amount at the surface. These effects might then affect the photostability of the drawn samples.

3.5. Accelerated photoaging of stabilized samples

To study the effect of the MDO process on the photostability of the PE-770-1 and PE-770-3 samples, accelerated photoaging experiments were performed in a SEPAP 12/24 device at 52 °C. The extent of photooxidation was assessed by FTIR transmission (Figs. 9a and 10a for the 1900–1500 cm^{-1} range; see also Figs. S6–9 for 3800–3100 and 1100–900 cm^{-1}) and UV–visible spectroscopies (Figs. 9b and 10b).

As seen from the FTIR results of both samples, the temperature at which the experiments were carried out (52°C) caused a re-solubilization of bloomed Tinuvin® 770 within the first hours of aging, as previously observed in Section 3.3. On a longer timescale,
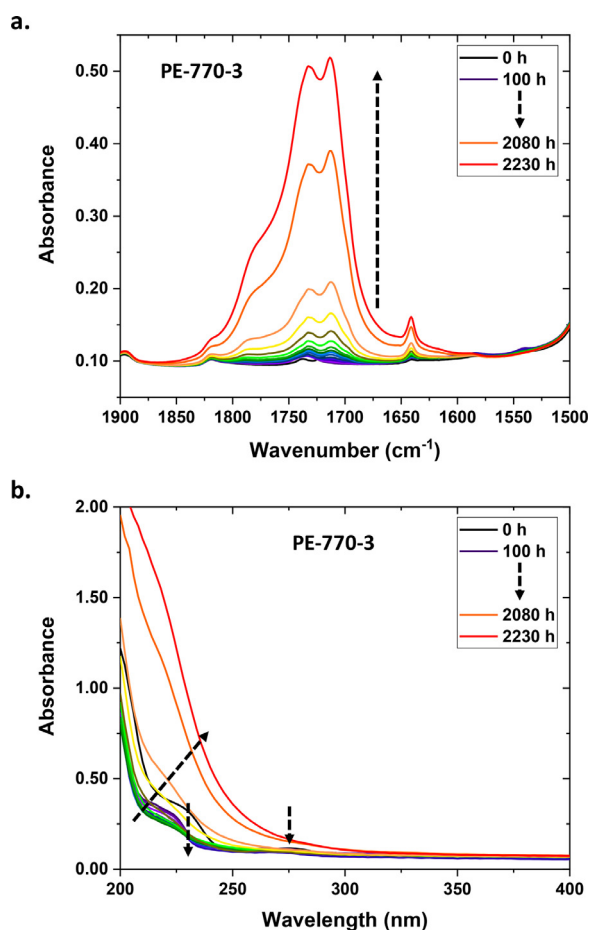
a.

b.

Fig. 10. a. FTIR transmission spectra in the 1900–1500 cm^{-1} region and b. UV–visible spectra of PE-770-3 after various photoaging durations. The arrows indicate the evolution with increasing UV exposure time.

the extent of polyethylene photooxidation can be followed through an increase in the intensity of absorption bands due to the appearance of oxidation products such as carboxylic acids (C=O stretching at 1713 cm^{-1}), hydrogen-bonded alcohols and hydroperoxides (O-H stretching at 3430 cm^{-1}) and vinyl groups (C-H bending at 909 cm^{-1}) [3,4,31]. The latter are due to the Norrish II reactions occurring for ketones upon UV irradiation. UV–visible spectra show the progressive disappearance of bands located at 230 and 275 nm, which are characteristic of the phenolic antioxidant in the polymer used for processing (also observed for pristine PE samples). No signal from Tinuvin® 770 was observed by UV–visible spectroscopy. Later, a growing absorption front in the UV region was observed, which was associated with the formation of oxidation products [4].

Usually, photooxidation kinetics are drawn from the absorbance measured by subtracting the spectrum before irradiation from the spectra recorded after UV exposure. However, in the present case, the absorbance value at 1713 cm^{-1} before UV exposure contains a nonnegligible contribution of the 1720 cm^{-1} absorption band of bloomed Tinuvin® 770, which has been shown to disappear through re-solubilization in the photoaging unit (*vide supra*). This will then distort the associated differential spectra. Therefore, ΔA values at 1713 cm^{-1} were measured by subtracting the absorbance after 100 h of UV exposure, when complete re-solubilization of the HALS stabilizer occurred (Figs. S10 and S11). Such an issue was not encountered for the two other bands characteristic of the oxidation products at 3430 and 909 cm^{-1} (Figs S12–15). The evolution of ΔA at 1713 cm^{-1} is plotted for PE-770-1 and PE-770-3 in Fig. 11 (see data for 3430 and 909 cm^{-1} in Figs S16 and S17). Fig. 10 also
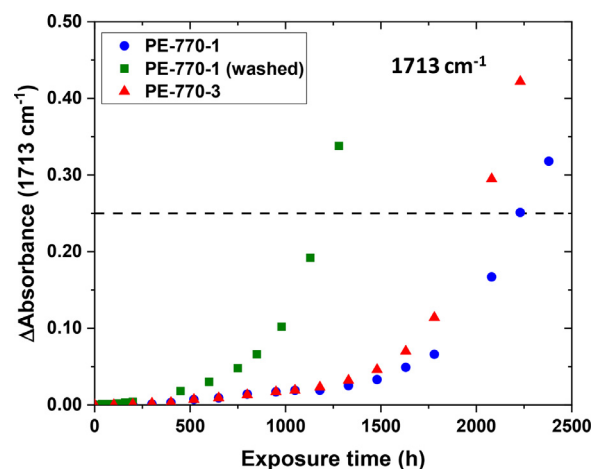

Fig. 11. Photoaging kinetics at 1713 cm^{-1} of PE-770-1 (blue circle), EtOH-washed PE-770-1 (green square) and PE-770-3 (red triangle). The dashed line indicates a value of $\Delta A = 0.25$. (For interpretation of the references to color in this figure legend, the reader is referred to the web version of this article.)

shows the kinetic curve for a PE-770-1 sample washed with EtOH before photooxidation (*vide infra*).

Photodegradation is faster for the drawn sample than for the undrawn sample. For instance, a ΔA value of 0.25 is reached in 2000 h for PE-770-3 *vs.* 2250 h for PE-770-1. A similar study was performed for undrawn (PE-1) and drawn (PE-3) pristine polyethylene (Fig. S18). This MDO process alone (with the morphological evolution it induces at the macromolecular scale) does not have such an effect on the photoaging kinetics of the unstabilized samples. As a consequence, the faster photodegradation observed for PE-770-3 is due to the loss of a large part of the bloomed stabilizer during MDO processing, which is not able to re-solubilize and prevent photooxidation. Because of the fast re-solubilization induced by the conditions of the accelerated photoaging experiment, the sample that contains the higher total (soluble and bloomed) amount of HALS is consistently better protected against oxidation (PE-770-1 in that case).

To illustrate the effect of re-solubilization on the photooxidation kinetics, a similar experiment was performed on a washed PE-770-1 sample (Fig. 11). The rate of formation of oxidation products is actually higher than that for the unwashed sample ($\Delta A = 0.25$ after 1200 h). This can be explained by the absence of the bloomed part of Tinuvin® 770 after washing, which cannot re-solubilize during the first hours of the photoaging experiment and prevent bulk oxidation of the polymer. This is an important result that unambiguously indicates that the re-solubilized form of Tinuvin® 770 is actually active for photostabilization.

4. Conclusion

Undrawn and MDO-drawn polyethylene samples stabilized by Tinuvin® 770 in conditions of supersaturation were studied. At room temperature, the stabilizer is present either in a soluble form within the polymer or in a precipitated form at the film surface as bloomed particles. This was confirmed by washing and heating experiments. For MDO-drawn samples with a draw ratio of 3, the total amount of Tinuvin® 770 was lower than that in the undrawn samples, whereas the amount of Tinuvin® 770 dissolved in the polymer was slightly higher. This means that the MDO process leads to a loss of bloomed Tinuvin® 770. Undrawn samples degrade faster than MDO-drawn samples during accelerated photoaging experiments performed at 52°C in a SEPAP 12/24 unit. The bloomed stabilizer can be dissolved in the polymer by increasing the temperature, which can explain the larger total amount (solu-

ble and bloomed) of Tinuvin® 770 in the undrawn samples. They are then better protected against oxidation during accelerated photoaging at higher temperatures. This was confirmed by the observation of faster oxidation kinetics for a sample washed prior to photooxidation to remove the bloomed HALS.

The reported results indicate that the bloomed stabilizer can be efficient and play a role as a stabilizer in the case of aging tests performed at temperatures higher than those encountered in natural weathering. The complete re-solubilization of bloomed Tinuvin® 770 at the temperature used in accelerated photoaging conditions (52°C in the SEPAP unit) points out a possible bias brought by increasing temperature when testing polymers with blooming stabilizers, in addition to the bias already reported (day and night cycles, seasonal variations, atmospheric pollution, etc.) [3]. Indeed, re-solubilization due to increasing temperature enhances the concentration of stabilizer within the polymer compared to its actual solubility at ambient temperature, which might affect the representativeness of accelerated photoaging compared to natural weathering. Moreover, the impact of rain during exposure to natural weathering could reduce the amount of bloomed stabilizer, as it can be progressively washed away from the surface. All these results emphasize that great care must be taken when dealing with blooming stabilizers in accelerated photoaging systems. As blooming HALS are generally used in association with non-migrating (*i.e.* polymeric) stabilizers, the effect of MDO processing on the solubility of such high molecular weight compounds and mixture of both kinds of additives would also be of great interest.

Declaration of Competing Interest

The authors declare that they have no known competing financial interests or personal relationships that could have appeared to influence the work reported in this paper.

CRediT authorship contribution statement

Julien Christmann: Investigation, Writing – original draft, Visualization. **Jean-Luc Gardette:** Writing – review & editing. **Gérard Pichon:** Resources. **Bruno Bouchut:** Resources. **Sandrine Therias:** Conceptualization, Supervision, Writing – review & editing.

Acknowledgements

Supplementary materials

Supplementary material associated with this article can be found, in the online version, at doi:10.1016/j.polymdegradstab.2021. 109683.

References

[1] A Rivaton, J-L Gardette, B Mailhot, Morlat-Therias S. Basic aspects of polymer degradation, Macromol. Symp. 225 (2005) 129–146.

[2] JF. Rabek, Polymer Photodegradation, Springer Science+Business Media, Dordrecht, 1995.

[3] JF. Rabek, Photodegradation of Polymers, Springer-Verlag, Berlin Heidelberg, 1996.

[4] M Gardette, A Perthué, J-L Gardette, T Janescka, E Földes, B Pukánszky, S. Therias, Photo- and thermal-oxidation of polyethylene: Comparison of mechanisms and influence of unsaturation content, Polym. Degrad. Stab. 98 (2013) 2383–2390.

[5] NC Billingham, PD Clavert, AS. Manker, Solubility of phenolic antioxidants in polyolefins, J. Appl. Polym. Sci. 26 (1981) 3543–3555.

[6] NC Billingham, PD Clavert, IW Okopi, A. Uzuner, The solubility of stabilizing additives in polypropylene, Polym. Degrad. Stab. 31 (1991) 23–26.

[7] HP Frank, H. Lehner, Distribution of ultraviolet stabilizers in crystalline polypropylene, J. Polym. Sci. C Polym. Symp. 31 (1970) 193–203.

[8] NC Billingham, PD. Calvert, Applications of ultraviolet microscopy to polymers, Dev. Polym. Char. 3 (1982) 229–259.

[9] J Malík, A Hrivík, E. Tomová, Diffusion of hindered amine light stabilizers in low density polyethylene and isotactlc polypropylene, Polym. Degrad. Stab. 35 (1992) 61–66.

[10] A Xu, S Roland, X Colin, Physico-chemical characterization of the blooming of Irganox 1076® antioxidant onto the surface of a silane-crosslinked polyethylene, Polym. Degrad. Stab. 171 (2020) 109046.

[11] A Xu, S Roland, X Colin, Physico-chemical analysis of a silane-grafted polyethylene stabilized with an excess of Iragnox 1076®. Proposal of a microstructural model, Polym. Degrad. Stab. 183 (2021) 109453.

[12] S Zehnacker, J. Marchal, IR spectrometric determination of concentrations of soluble and insoluble fractions of bis(2,2,6,6-tetramethyl-4-piperidinyl) sebacate in polymers: application to LDPE films, Polym. Degrad. Stab. 45 (1994) 435–439.

[13] Y Qing, X Wenying, B. Rånby, Photoinitiated crosslinking of low density polyethylene. III: Degradation and stabilization of photocrosslinked polyethylene, Polym. Eng. Sci. 34 (1994) 446–452.

[14] NS Allen, J-L Gardette, J Lemaire, A comparative study of structure and polymer effects on the photo-stabilising activity of hindered piperidine light stabilisers, Polym. Degrad. Stab. 8 (1984) 133–144.

[15] DR Breese, E. Hatfield, KL In Yam, in: The Wiley Encyclopedia of Packaging Technology, third ed., Wiley, Hoboken NJ, 2009, p. 685.

[16] E. Hatfield, in: Multilayer Flexible Packaging, second ed., Elsevier, Oxford, 2016, p. 147.

[17] A Bafna, D McFaddin, G Beaucage, J Merrick-Mack, FM. Mirabella, Integrated mechanism for the morphological structure development in HDPE melt-blown and Machine-Direction-Oriented films, J. Polym. Sci. B 45 (2007) 1834–1844.

[18] E Hatfield, R Tate, K Williams, W. Todd, New MDO medium molecular weight high density polyethylene films, J. Plast. Film Sheeting 18 (2002) 117–127.

[19] SH Tabatabaei, L Parent, P Cigana, A Ajji, PJ. Carreau, Effect of Machine Direction Orientation conditions on properties of HDPE films, J. Plast. Film Sheeting 25 (2009) 235–249.

[20] T Chatterjee, R Patel, IV J Garnett, R Paradkar, S Ge, L Liu, KT Forziai Jr, Shah N, Machine Direction Orientation of high density polyethylene (HDPE): barrier and optical properties, Polymer 55 (2014) 4102–4115.

[21] S Srinivas, P Brant, Y Huang, DR. Paul, Structure and properties of oriented polyethylene films, Polym. Eng. Sci. 43 (2003) 831–849.

[22] JH. Schut, MDO films: lots of promise, big challenges, Plast. Technol. (2021) available online at https://www.ptonline.com/articles/mdo-films-lots-of-promise-big-challenges (consulted on the 01/02/).

[23] V Ratta, GL Wilkes, TK. Su, Structure-property-processing investigations of the tenter-frame process for making biaxially oriented HDPE film. I. Base sheet and draw along the MD, Polymer 42 (2001) 9059–9071.

[24] DR Breese, G. Beaucage, Modelling the mechanical properties of highly oriented polymer films: a fibre/gel composite theory approach, J Polym Sci B 46 (2008) 607–618.

[25] JY. Moisan, Diffusion des additifs du polyéthylène – III. Influence de l'orientation, Eur. Polym. J. 16 (1980) 997–1002.

[26] BorShape™ FX 1001 Product Data Sheet, Borealis, 2012.

[27] J Lemaire, R Arnaud, J-L Gardette, JM Ginhac, T Ly, E. Fanton, Vieillissement des polymères: empirisme ou science? Caoutchoucs Plast. 593 (1979) 147–152.

[28] DA Skoog, FJ Holler, SR. Crouch, Principles of Instrumental Analysis, sixth ed., Thomson Brooks/Cole, Belmont, 2007.

[29] J Brandrup, EH Immergut, EA. Grulke, Polymer Handbook, fourth ed., Wiley, New-York, 1999.

[30] B. Wunderlich, Thermal Analysis of Polymeric Materials, Springer-Verlag, Berlin Heidelberg, 2005.

[31] G. Socrates, Infrared and Raman Characteristic Group Frequencies, third ed., Tables and Charts, Chichester: Wiley, 2001.

[32] O Vedal, OH Ellestad, P. Klaboe, The vibrational spectra of piperidine and morpholine and their N-deuterated analogues, Spectrochim. Acta 32A (1976) 877–890.

[33] E Górnicka, JE Rode, ED Raczyńska, B Dasiewicz, Dobrowolski JCz, Epxerimental (FT-IR and Raman) and theoretical (DFT) studies on the vibrational dynamics in cytisine, Vibr. Spectrosc. 36 (2004) 105–115.